J Braz. Soc. Mech. Sci. Eng. (2017) 39:2289–2306
DOI 10.1007/s40430-016-0671-y

TECHNICAL PAPER

Thermal analysis of solar-assisted heat pumps for swimming pool heating

Allan R. Starke[1] · Jose M. Cardemil[2] · Rodrigo Escobar[3] · Sergio Colle[1]

Received: 1 August 2016 / Accepted: 4 November 2016 / Published online: 21 November 2016

Abstract The present work analyzes the technical feasibility of solar-assisted heat pumps for swimming pool heating in South Brazil. The methodology is based on computer simulations for four configurations of heating systems for private outdoor pools that are located in Florianopolis, SC, Brazil. The simulations were performed using TRNSYS software. The four configurations considered herein include a conventional heat pump in which ambient air is used as the heat source for an air-to-water heat pump (ASHP), a parallel configuration between the solar collectors and an air-to-water heat pump (SA-ASHP), a series configuration in which the solar collectors are used as the heat source for a water-to-water heat pump (SA-WSHP), and a combination of the last two systems (SA-DSHP). The simulation results indicate that the solar-assisted heat pump systems can achieve a significantly better performance than a conventional heat pump system. The proposed schemes can reduce energy consumption up to 48%, and the systems can achieve a seasonal performance factor between 6.7 and 8.2. Therefore, a proper design of the solar field is determined through a detailed economic assessment by combining the cost and performance of all of the system components. However, the results of the evaluation shows that only SA-ASHP and SA-DSHP are economically feasible.

Keywords Swimming pool heating · Solar energy · Solar-assisted heat pump · TRNSYS · Brazil

Technical Editor: Jose A. dos Reis Parise.

✉ Allan R. Starke
allan.starke@lepten.ufsc.br

[1] LEPTEN-Laboratory of Energy Conversion Engineering and Energy Technology, Department of Mechanical Engineering, Federal University of Santa Catarina, Florianopolis, Brazil

[2] Department of Mechanical Engineering, Universidad de Chile, Beauchef 851, Santiago, Chile

[3] Mechanical and Metallurgical Engineering Department, Pontificia Universidad Católica de Chile, Santiago, Chile

Nomeclature

Abbreviations

AS	Air source
ASHP	Air source heat pump
CAP	Capacity
COP	Coefficient of performance
DX-SAHP	Direct expansion solar-assisted heat pump
FINA	International Swimming Federation
HP	Heat pump
IAM	Incident angle modifier
IEA	International Energy Agency
i-SAHP	Indirect solar-assisted heat pump
LCS	Life cycle savings
PWR	Power
SA-ASHP	Solar-assisted air source heat pump
SA-DSHP	Solar-assisted dual source heat pump
SAHP	Solar-assisted heat pump
SA-WSHP	Solar-assisted water source heat pump
SF	Scale factor
SPF	Seasonal performance factor
TMY	Typical meteorological year
TXV	Thermostatic expansion valve
WS	Water source

List of symbols

C	Constant, coefficient, cost
C_F	Fuel tariff

$C\bar{O}P$	Seasonal coefficient of performance
C_p	Specific heat
d	Discount rate
F	Fraction, ration, Free-energy fraction
G	Irradiation
$\bar{h}$	Convection heat transfer coefficient
I	Inflation rate
$\dot{m}$	Mass flow rate
M_s	Insurance and maintenance cost
N_e	Period of economic analysis
P	Pressure
Q	Energy
$\dot{Q}$	Heat flow
R_v	Resale value
T	Temperature
v	Specific volume
W	Energy from work
w	Wind speed
z	Height

Greek symbols

α	Evaporation heat transfer coefficient, absorptance
β	Collector slope
ΔT	Temperature difference
ϵ	Emissivity of water surface
η	Efficiency
κ	Isentropic exponent
$\dot{v}$	Volumetric displacement rate
ϕ	Humidity
ρ	Specific mass

Subscript

0	Sea level
A	Area dependent
amb	Ambient
AS	Air source heat pump
ashp	Air source heat pump
aux	Auxiliary
c	Condenser
col	Collector
conv	Convection
cv	Clearance volume
direct	Direct
e	Evaporator
ele	Electricity
evap	Evaporation
F	Fuel
fr	Freshwater
glob	Global
hp	Heat pump
in	Inlet flow
inst	Installation
L,l	Load
leak	Leakage
out	Outlet flow
p	Pool
rad	Long-wave radiation
set	Set point
sh	Super-heating
sky	Sky
st	Saturation
sun	Short-wave radiation, solar
surr	Surroundings
valve	Valve
w	Water
WS	Water source
wshp	Water source heat pump

1 Introduction

Brazil has the second largest swimming pool market in the world, and this market increases by approximately 5% each year. In the southern and southeastern regions of Brazil where the hot season lasts from December to March, it is necessary to use auxiliary heating devices so that consumers can use their pools year round.

According to FINA (International Swimming Federation) facility rules, the water temperature should be maintained between 25 and 28 ℃ for standard and Olympic competition pools [9], while the American Red Cross recommends a pool water temperature of 25.5 ℃ for fitness swimming and 27 ℃ for recreational swimming [1]. Although the water temperature in home pools is defined according to individual preferences, these values serve as a guide for human health, care, and comfort.

A recent analysis of the energy data for the 11 IEA member countries between 1974 and 2010 showed that the improvements in energy efficiency during this period allow to ,hypothetically, avoid an energy consumption of approximately 65% of the 2010 total energy consumption [13]. This shows how large the potential is for cost-effective energy savings without compromising the standard of living. One example of this potential is the European Union's 2012 Energy Efficiency Directive [8], which sets a strategy for achieving its target of 20% primary energy savings by 2020. Based on these energy efficiency requirements, it is natural to use heat pumps or solar systems to heat swimming pools with lower energy consumption than alternative methods. Although these systems have lower operation costs, their performance is highly dependent on the weather conditions. Therefore, in some cases, they may not be able to supply the heating demand.

The combined use of heat pumps and solar collectors can reduce several of the disadvantages that these systems

present when they operate separately [5]. For instance, during the winter, solar collectors provide water with temperatures that are too low for direct heating, but they can nevertheless be used as a heat source for a heat pump, as shown by [10]. In addition, solar systems exhibit higher efficiency when operated at low temperatures, thus enabling the use of uncovered and less expensive options such as polymeric collectors. Hence, combining both systems may compensate for the decrease in the performance of conventional solar systems on cloudy days and for the low heating capacity of heat pumps on cold days. Solar collectors can be connected in series to a water-to-water heat pump and can also operate as the heat source for this device [18]. Another configuration involves connecting the solar collectors in parallel with an air source heat pump. Finally, both configurations can also be combined to configure a solar-assisted dual-source heat pump.

Several studies have analyzed the utilization of solar collectors for swimming pool heating. In short, [11] developed and validated a computational model for simulating the thermal behavior of a swimming pool compatible with TRNSYS software. Recently, [22] validated this TRNSYS model for a private open-air pool with a $50m^2$ surface. These authors concluded that the Richters correlation used for the evaporative losses showed the best agreement for the pool temperature and, therefore, they recommended the use of this correlation.

Solar-assisted heat pumps have been studied by many researchers over the past several decades. A comprehensive review of this topic was performed in [12, 19] and [4]. According to these references, SAHP systems are commonly classified into two main types of systems: direct expansion solar-assisted heat pumps (DX-SAHP) and indirect solar-assisted heat pump (i-SAHP). DX-SAHP uses a two-phase flow solar collector to directly evaporate the refrigerant fluid of the vapor compression cycle. Therefore, the cooler temperature of the solar collector allows us to develop a higher efficiency on the absorption of solar radiation and, consequently, this system could achieve a higher overall performance, as later demonstrated by [24]. In contrast, in i-SAHP, the solar water loop is connected to the evaporator of a water source heat pump. Hence, the refrigerant fluid is evaporated in a heat exchanger. The main advantages of i-SAHP versus DX-SAHP are the possibility of using commercial water source heat pumps, allowing the use of cheap unglazed collectors and configuring a bypass to the heat pump to supply the heat load directly [25]. Meanwhile, i-SAHP presents higher plant costs and the inherent inefficiencies of the intermediate water-refrigerant heat exchanger, which could lead to a significant reduction in the overall performance. The use of water in a collector's circuit with commercial equipment is a more suitable solution for the Brazilian market based on the experience of the currently available workforce. Therefore, the use of i-SAHP was considered for this study.

Regarding the use of SAHP for pool heating, [24] investigated i-SAHP for indoor swimming pool heating in Italy. The performance of the system was analyzed for a fixed thermal load by considering different climatic conditions such as ambient temperature, solar irradiance, and degree-days. Chow et al. [3] studied the performance of i-SAHP for indoor pool water supply and swimming hall space heating. Through the TRNSYS simulation environment, the dynamic performance was evaluated based on the wintertime operation schedule of a public swimming center located in Hong Kong. The system achieved a mean heating COP of 4.52 and a global fractional energy savings factor of 79%. The authors showed that the proposed system has an economic payback period of less than 5 years under the specific conditions considered for that study.

From the literature review, it appears that the main applications of SAHP are space heating and domestic hot water, while the use of this device for swimming pool heating is restricted to indoor pools. Therefore, this study proposes a methodology for analyzing the energy-savings potential of i-SAHP for outdoor swimming pool heating by simulating four different configurations.

The main objectives of this work is to develop a methodology for simulating different configurations of swimming pool heating systems, using solar-assisted heat pumps, in the transient regime, allowing to assess their performance in terms of energy consumption and solar contribution.

The four heating systems studied are: an air source heat pump system (ASHP, Fig. 1a), which is also considered the reference case; a parallel system or solar-assisted air source heat pump system (SA-ASHP, Fig. 1b) in which the solar collectors are connected in parallel to an air source heat pump; the series system or solar-assisted water source heat pump system (SA-WSHP, Fig. 1c) in which the collectors are connected in series to a water-to-water heat pump; and a dual-source heat pump system (SA-DSHP, Fig. 1d) in which the heat pump has two evaporators (one connected in series to the solar collector and the other is an air source evaporator).

2 Mathematical models

The methodology used was adapted from the methodology developed by the Solar Energy Laboratory at the University of Wisconsin-Madison [20]. The Transient System Simulation Program-TRNSYS [15] was used to perform the simulations of the complete system, where each component was simulated using a TRNSYS module (Type). Currently, there is no TRNSYS type for simulating the thermodynamic cycle of a heat pump based on coupled heat transfer,

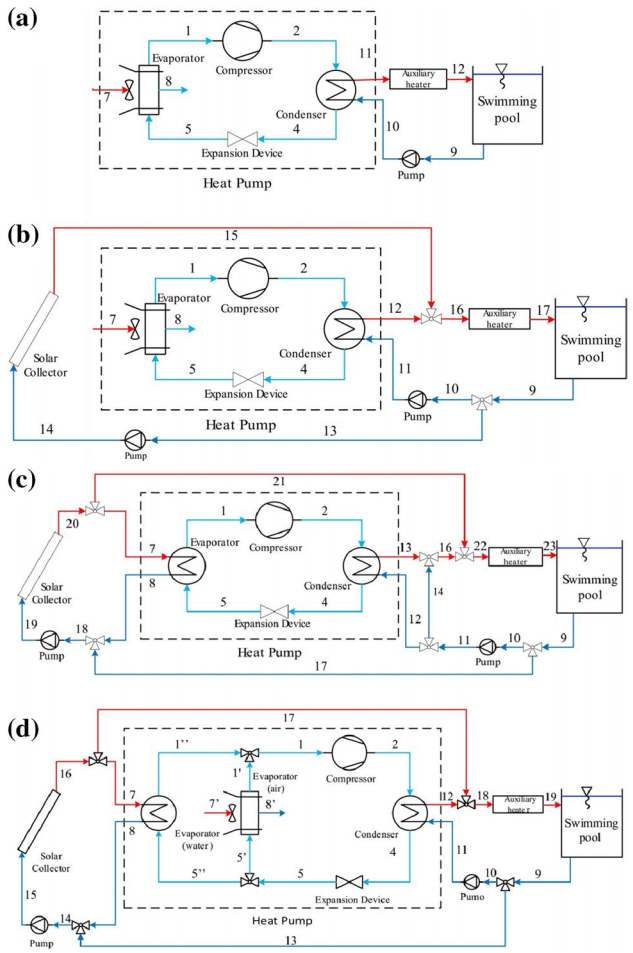

Fig. 1 Schematic diagram of the **a** ASHP, **b** SA-ASHP, **c** SA-WSHP and **d** SA-DSHP systems

mass and energy equations. Thus, the simulation was conducted using a performance matrix, because all of the types developed for conditioning equipment are performed in the TRNSYS environment. This performance matrix was estimated by a thermodynamic model of a heat pump developed using Engineering Equation Software [16]. The TRNSYS standard library contains types that model most of the components of the systems studied herein (e.g., solar collector, pumps, valves, and controllers). The exception is the swimming pool for which an additional type based on the model of an external pool developed by [11] was implemented as an add-on.

2.1 Solar collectors

Simplified models based on empirical characteristics are commonly employed to simulate transient solar collector performance. In this study, an uncovered polymeric solar collector was considered and, consequently, there was no need to include the incidence angle modifier (IAM) in the efficiency calculations. Thus, the TRNSYS Type 1a (Quadratic Efficiency Collector–No Incident Angle Modification) module was employed. This module is based on the quadratic instantaneous efficiency equation, as indicated by [7],

$$\eta_c = F_{\mathrm{R}}(\tau\alpha)_n - F_{\mathrm{R}}U_{\mathrm{L}}\frac{(T_{\mathrm{col,i}} - T_{\mathrm{amb}})}{G_{\mathrm{T}}} - F_{\mathrm{R}}U_{\mathrm{LT}}\frac{(T_{\mathrm{col,i}} - T_{\mathrm{amb}})^2}{G_{\mathrm{T}}} \quad (1)$$

where G_{T} is the total incident solar radiation on the collector plane, F_{R} the heat removal factor, $(\tau\alpha)_n$ the effective transmittance–absorptance product normal to the collector, U_{L} is the overall heat loss coefficient, U_{LT} is the correction factor of the overall heat loss coefficient, $T_{\mathrm{col,i}}$ is the inlet water temperature in the collector, and T_{amb} is the ambient temperature.

The efficiency parameters of the collector were experimentally determined. The numeric values are $F_{\mathrm{R}}(\tau\alpha)_n = 0.7327$, $F_{\mathrm{R}}U_{\mathrm{L}} = 19.3$ W/(m^{2}K), and $F_{\mathrm{R}}U_{\mathrm{LT}} = 0$ [26]. The mass flow rate under the test conditions was $\dot{m}_{\mathrm{test}} = 0.0182$ kg/(m^{2}s), and the solar collector has an aperture area of 1.1 m^2.

2.2 Heat pump

A physical deterministic model was applied in combination with an equation-fitting procedure that is used to evaluate the performance of each component of the cycle. For example, the thermodynamic performance of a compressor can be evaluated by an isentropic efficiency approach, or could also be evaluated by an equation-fit model as a function of the boundary conditions, i.e., external fluid mass flow rate and temperatures, as suggested by [14]. In addition, a parameter estimation method was used to calculate the parameters of the internal components. To do so, a multivariable optimization process was employed to estimate these parameters, and then those values were used as inputs to simulate the performance of the equipment using different boundary conditions.

The parameter estimation for the base model was developed to generate a performance matrix that can be used on TRNSYS environment to simulate the performance of the heat pump in terms of three independent variables, e.g., ambient temperature, water temperature, and mass flow rate. A generic module was used to read the data from an external file and then to estimate the performance of the device, depending on the operating conditions. The standard TRNSYS module that is most suitable for completing this procedure is Type 42-(Conditioning Equipment).

The choice of a parameter estimation-based model was adopted for three main reasons: first, there is limited commercial information available in Brazil regarding

water-to-water or air-to-water heat pumps; therefore, it is not feasible to use a detailed model that requires a parameter from the internal components. In addition, although there are some catalogs for water-to-water heat pumps, the data reported consider only a few points close to the boundary conditions observed in solar heating systems for pools. The second reason is that the use of a detailed model allows not only the extrapolation of data—which is important in energy calculations and/or building simulations—but also scaling the equipment in a deterministic and physically consistent way. Finally, there is no information or catalog data available for the dual-source heat pump. However, a performance matrix can be generated using a simulation tool for water-to-water and air-to-water heat pumps, whereas the input parameters for the compressor, expansion valve, and condenser are the same for both heat pump types.

The mathematical model was implemented in the well-known equation-solving program EES [16], whereas the parameter estimation process was accomplished using a multivariable optimization method that is already implemented in EES. The following assumptions were considered to simplify the model:

- The cycle is assumed to strictly operate in a steady state.
- The pressure drop through the working fluid lines is neglected. Hence, the cycle operates at only two pressure levels.
- There are no isenthalpic effects on refrigerant properties and compressor operation.
- The degree of superheating is controlled by a thermostatic expansion valve.
- No degree of sub-cooling was considered in the condenser.
- No thermal losses are considered in the pipes, compressor, expansion device, or heat exchangers.
- The effects of oil in the thermodynamic properties of the fluid were neglected.
- The isentropic index is dependent on the refrigerant and is calculated at the compressor inlet.

2.2.1 *Component modeling*

Each component of the heat pump is modeled by fundamental mass and energy equations and specific governing equation, which are presented in this section.

The performance of the compressor is described by assuming a constant isentropic efficiency, which is set as an input parameter of the model. However, the capacity performance of the compressor is described in terms of the volumetric efficiency as suggested by [6],

$$\eta_{\text{vol}} = C_{\text{leak}}\left[1 - C_{\text{cv}}[P_2/P_1]^{1/\kappa}\right] \quad (2)$$

where P_1 and P_2 are the pressures at the inlet and outlet of the compressor, respectively, and κ is the isentropic exponent approximated as the heat capacity ratio at the inlet state of the compressor. Constants C_{leak} and C_{cv} are input parameters and are associated with leakage and the clearance volume, respectively. The volumetric efficiency is used to calculate the refrigerant mass flow rate flowing throughout the compressor, as $\dot{m}_{\text{refri}} = \eta_{\text{vol}}\dot{v}/v_1$, where $\dot{v}$ is the volumetric displacement rate of the compressor and v_1 is the specific volume at the compressor inlet.

The electric power required by the compressor is determined by applying the first law of thermodynamics and a mechanic-to-electric efficiency. Hence, the electrical power of the water-to-water heat pump is equivalent to the electrical power of the compressor. For the air-to-water heat pump, the electric power is the sum of the electric power consumed by the compressor and the power used at the evaporator fan, which is estimated using a linear fit of data of a ventilator manufacturer.

For both heat exchangers (i.e., evaporator and condenser) a moving-boundary or zone model was applied, based on the location where the phase transition occurs, as suggested by [21]. Each subdivision is evaluated using the ϵ-NTU model. For the water–water heat pump, a counterflow heat exchanger is considered for the condenser and the evaporator. A counterflow heat exchanger is also considered for the condenser of the air–water heat pump, and a crossflow heat exchanger is considered for the evaporator.

Regarding the expansion device, a globally linear thermostatic expansion valve (TXV) model is considered [17]. In this model, TXV automatically adjusts the valve opening based on the superheating of the refrigerant at the evaporator outlet. Thus, the mass flow rate through TXV is expressed as follows,

$$\dot{m}_{\text{refri}} = C\left[\frac{(\Delta T_{\text{sh,operaing}} - \Delta T_{\text{sh,static}})}{(\Delta T_{\text{sh,rating}} - \Delta T_{\text{sh,static}})}\right]\sqrt{\rho_4(P_4 - P_5)} \quad (3)$$

where ρ_4 is the specific mass at the valve inlet and P_4 and P_5 are the pressures at the valve inlet and outlet, respectively. $\Delta T_{\text{sh,operating}}$ is the degree of superheating at a current operation condition; $\Delta T_{\text{sh,static}}$ is the static degree of superheating and represents the degree of superheating at which the valve starts to open; $\Delta T_{\text{sh,rating}}$ is the degree of superheating at the rating condition; and C represents the valve flow coefficient. Typically, the parameters $C/(\Delta T_{\text{sh,rating}} - \Delta T_{\text{sh,static}})$ are provided by the valve manufacturers. Therefore, these three parameters are defined as a known input for the model.

A commercial water source heat pump was considered as a reference for the parameter estimation process. This heat pump has a nominal heating capacity of 12.9 kW and uses R-410A as the refrigerant fluid [27]. This model was

selected because it represents an average capacity in the range for residential equipment.

Power consumption and heating capacity calculated by the model can be compared with catalog performance data. Then, it is possible to evaluate the relative error between the model results and the catalog data. Considering that this relative error should be small, it is possible to find a minimum value as a function of the model parameters.

The model quantities of interest are in good agreement with the data from the catalog. The model agrees with the catalog data within ±3% of error. These results are in accordance with [14]. In addition, the coefficient of determination (R^2) has a value of 0.995 for the heating capacity and a value of 0.972 for the electrical power consumption, which are in agreement with the values obtained by [28].

2.3 Swimming pool

The model proposed by [11] was used to perform the transient simulation of the swimming pool. The Type 144 model (Indoors and Outdoors Swimming Pool Model) allows for the evaluation of the water temperature and the heat fluxes between the pool and the surroundings. In this model, the following heat fluxes were considered: heat flow rate by evaporation ($\dot{Q}_{\text{evap}}$), heat flow rate by convection ($\dot{Q}_{\text{conv}}$), heat flow rate by short-wave radiation ($\dot{Q}_{\text{sun}}$), heat flow rate by long-wave radiation ($\dot{Q}_{\text{rad}}$), heat loss due to freshwater supply ($\dot{Q}_{\text{fr}}$), and heat flow rate from the heating device ($\dot{Q}_{\text{aux}}$). The thermal conduction to the ground was neglected because it represents a minor influence on the overall energy flow and is difficult to estimate properly, as noted by [2]. The water in the pool was fully mixed; therefore, the pool water temperature (T_{p}) can be calculated as follows,

$$\rho_w C_{p,w} V_p \frac{\mathrm{d}T_{\text{p}}}{\mathrm{d}t} = \sum \left(\dot{Q}_{\text{in}} - \dot{Q}_{\text{out}}\right) \tag{4}$$

where ρ_w and $C_{p,w}$ are the specific mass and specific heat of water, while V_{p} is the pool volume (control volume) and $\dot{Q}_{\text{in}}$ and $\dot{Q}_{\text{out}}$ are the heat flow rates entering and leaving the control volume.

The evaporation heat loss was estimated by an empirical correlation in which the driving force is the difference between the vapor pressures evaluated at the water surface and the ambient surroundings. Hence, it was assumed that the temperature in the layer above the water surface was the same as the pool temperature (T_{p}) and had a relative humidity level of 100%; thus, the evaporative heat flux can be calculated by the following expression,

$$\dot{Q}_{\text{evap}} = A_{\text{p}} \alpha_{\text{evap}} \left(P_{\text{w,sat}}(T_P) - P_{\text{st,amb}}(T_{\text{amb}})\right) \tag{5}$$

where A_{p} is the area of the pool water surface, $P_{\text{w,sat}}$ the saturation pressure in the layer above the water surface, and $P_{\text{st,amb}}$ the vapor pressure under ambient conditions and can be calculated by $P_{\text{st,amb}}(T_{\text{amb}}) = \phi_{\text{amb}} P_{\text{w,sat}}(T_{\text{amb}})$, in which ϕ_{amb} is the ambient relative humidity. The evaporative heat transfer coefficient can be calculated by the following empirical expression,

$$\alpha_{\text{evap}} = 42.29 + 56.52 w^{0.5} \tag{6}$$

where w is the wind speed, in m/s, at a height z. The wind speed indicated by weather data w_0 is measured at a height of 10 m (z_0). This value shows large differences with respect to the values measured close to the water surface. In this context, [2] suggested a correction factor to calculate the wind speed at a desired height as a function of the measurements collected at 10 m,

$$w = w_0 (z/z_0)^{(1/F_{\text{surr}})} \tag{7}$$

where F_{surr} is a surrounding factor for which a value of 10 was considered in this study, as recommended for free water surfaces.

The heat flow by convection is defined by the commonly used expression $\dot{Q} = \bar{h} A_{\text{p}} (T_{\text{p}} - T_{\text{amb}})$, where for the purpose of this study, the expression for the convection heat transfer coefficient ($\bar{h}_{\text{conv}}$) proposed by Czarnecki apud [2] was considered,

$$\bar{h}_{\text{conv}} = 3.1 + 4.1 w \tag{8}$$

The wind speed for this correlation must be corrected using Eq. 7 for a height of $z = 3$ m. The short-wave heat flow is calculated from the total solar radiation on a horizontal surface,

$$\dot{Q}_{\text{sol}} = \alpha_p A_{\text{p}} G_{\text{glob}} \tag{9}$$

where α_p is the effective absorptance and G_{glob} is the global irradiance on the horizontal. Studies have demonstrated that the pool depth and the incident angle of solar radiation have a small effect on α_p, the value of which is typically greater than 0.8 [11]. In this study, a value of $\alpha_p = 0.9$ was assumed.

The heat flow rate by long-wave radiation can be calculated using the Stefan–Boltzmann law. For outdoor pools, radiative exchanges between the pool water surface and the sky at an effective sky temperature T_{sky} are considered. Hence, the heat flow rate is given as follows,

$$\dot{Q}_{\text{rad}} = \epsilon_w A_p \sigma (T_p^4 - T_{\text{sky}}^4) \tag{10}$$

where the water surface emissivity ϵ_w is a constant equal to 0.9 [2]. The effective sky temperature can be calculated using a specific function in TRNSYS (Effective Sky Temperature) [15].

Finally, to maintain a constant swimming pool volume, it is necessary to replace the water lost by evaporation. The amount of heat and mass lost by this phenomenon can be determined by applying the first law of thermodynamics for energy and mass balances ($\dot{Q}_{fr}$). Analogously, a simple energy balance within the component obtains the heat flow rate of the heating system ($\dot{Q}_{aux}$).

3 Performance analysis

The thermal performance of the systems analyzed herein is assessed by means of an annual simulation, considering a transient model using a 6-min time step. For this purpose, some additional parameters are necessary versus those defined in the previous section. For instance, the collector array consisted of five rows with ten identical solar collectors (1.1 m^2) connected in series and oriented facing the equator with a slope angle equal to the latitude plus 10 degrees ($\beta = 37.6°$). All configurations also include an auxiliary heater to ensure that the swimming pool temperature is maintained between 24 and 28 °C.

For SA-ASHP, the water mass flow rate through the collectors was calculated as a function of the total area of the solar field and the test mass flow rate. Meanwhile for the SA-WSHP, the mass flow rate through the collectors is assumed equivalent to the minimal flow rate admissible at the water source heat pump evaporator (0.6 kg/s).

A maximum power of 30 kW was specified for the auxiliary heater. However, the actual power is modulated to ensure an outlet water temperature of 35 °C. The efficiency of the device and the specific fuel for its operation were not considered in this study, because the focus is on the assessment of the contribution of the solar-assisted heat pump.

The meteorological data for Florianópolis were introduced using a TMY database that was available from [23]. Florianópolis has a warm humid subtropical climate, with distinct seasons of the year—well-defined summer and winter. The monthly average values of irradiation, temperature and humidity are presented in Table 1. On the other hand, the main design parameters and the parameters of the reference case are summarized in Table 2.

3.1 Performance indicators

The thermal performance of each configuration was measured in terms of the fraction of the total load met by non-purchased energy or "free-energy fraction", as defined by [10],

$$F = 1 - (W_{hp,ele} + Q_{aux})/Q_L \tag{11}$$

where $W_{hp,ele}$ is the electric energy consumed by the heat pump, Q_{aux} the energy consumed by the auxiliary heater and Q_L the pool thermal load, which is equivalent to the energy delivered by the heat pump, the auxiliary heater, and the bypass circuit. It is worth noting that the thermal performance fraction (F) only represents an energy requirement; hence, it does not distinguish between different types of fuels. To identify these differences, Eq. (11) can be rewritten as follows,

$$F = 1 - \frac{W_{hp,ele}}{Q_L} - \frac{Q_{aux}}{Q_L} = 1 - F_{hp} - F_{aux} \tag{12}$$

where F_{hp} represents the ratio between the energy consumed by the heat pump and the overall pool thermal load. Similarly, F_{aux} represents the ratio between the energy consumed by the auxiliary heater and the pool thermal load. Therefore, these ratios represent the fractions of the energy consumed by the heat pump and the auxiliary heater, respectively. The energy delivered by the auxiliary heater is equivalent to the energy consumed by the equipment, because only the energy requirements are considered in this study. Nonetheless, the efficiency developed for different types of heater or even different fuels could be considered in a post-processing procedure.

The energy load fraction of the direct solar heating operation mode can be defined as,

$$F_{l,direct} = \frac{Q_{l,direct}}{Q_L} \tag{13}$$

where $Q_{l,direct}$ is the energy delivered to the pool by the solar field when the bypass heating mode in enabled. Thus, the energy load fraction of the heat pump is obtained by

$$F_{l,wshp} = \frac{Q_{c,wshp}}{Q_L} \tag{14}$$

$$F_{l,ashp} = \frac{Q_{c,ashp}}{Q_L} \tag{15}$$

where $Q_{c,wshp}$ and $Q_{c,ashp}$ are the amounts of thermal energy delivered to the pool by the condenser of the water-to-water and air-to-water heat pumps, respectively. For the dual-source heat pump, these variables represent the energy delivered to the pool by the condenser when the equipment operates using the water evaporator and the air evaporator, respectively.

The seasonal performance of the heat pump is evaluated in terms of the seasonal COP, defined as follows:

$$\overline{COP} = \frac{Q_c}{W_{hp,ele}} \tag{16}$$

where Q_c is the energy delivered by the condenser of the heat pump and $W_{hp,ele}$ is the electricity consumed by the equipment.

Finally, the seasonal performance factor of the whole system is defined as follows:

Table 1 Climatological and irradiation characteristics of Florianópolis

	Monthly average of daily irradiation on horizontal (MJ/m^2)			Ambient temperatures (°C)			Monthly average humidity (%)
	Global	Direct	Diffuse	High	Mean	Low	
Jan	20.4	9.3	11.1	34.1	25.3	20.3	78.2
Feb	19.9	11.7	8.1	32.6	25.0	17.5	87.6
Mar	15.9	7.6	8.4	34.7	24.2	15.4	83.8
Apr	14.0	7.9	6.0	30.8	22.7	13.4	77.9
May	12.4	8.8	3.7	31.2	19.2	12.3	81.4
Jun	10.5	5.5	5.1	31.0	18.7	8.9	74.3
Jul	9.7	5.6	4.1	30.2	18.5	10.5	82.7
Aug	12.8	7.0	5.8	30.6	17.0	7.9	77.4
Sep	13.4	5.4	8.0	34.0	18.9	11.0	80.5
Oct	15.3	7.3	8.0	30.3	20.5	15.0	82.7
Nov	20.7	11.1	9.6	31.4	21.7	14.6	84.7
Dec	23.5	13.3	10.2	35.3	24.2	16.4	80.2

Table 2 Reference system's main design parameters.

Parameter	Value
Main design	
Location	Florianópolis/Brazil (27.6°S/48.5°W)
Design pool temperature	24–28°C
Pool water volume	36 m^3
Pool water surface	24 m^2
Collector slope	$\beta = 37.6°$
Collector type	Polymeric
Reference case	
Field aperture area	55 m^2
AS nominal heat capacity	9.7 kW
WS nominal heat capacity	11.87 kW
DS nominal heat capacity (air/water)	9.7/11.87 kW

$$\mathrm{SPF} = \frac{Q_\mathrm{L}}{W_\mathrm{hp,ele} + Q_\mathrm{aux}} \tag{17}$$

This indicator shows how efficient the system operates, when considering the contribution of solar energy. Therefore, Eq. (11) can be rewritten as follows:

$$F = 1 - \mathrm{SPF}^{-1} \tag{18}$$

It is important to highlight that these quantities are integrated over a year or a month, so they indicate annual or monthly fractions.

4 System simulation

The simulations described herein consider an outdoor pool without a cover, located in Florianópolis, Brazil, with the features described in Table 2. Considering the lower values of ambient temperature during the night and the absence of solar radiation during this period, it is possible to infer that the thermal load profile of the swimming pool will show consumption after dawn and during the night, which is not correlated with the availability of solar energy. Nonetheless, for domestic applications, it is probably unnecessary to heat the pool during the early morning period. Therefore, in this study, two set-point temperature schedules were considered to control the pool temperature, as depicted in Table 3.

All four systems are controlled by an N-stage thermostat controller. The set-point temperatures and the corresponding dead bands are listed in Table 4. A higher value of the set point for direct solar heating was assumed to avoid oscillations on the control signals for the solar field pump. On the other hand, a lower value for the auxiliary heater was assumed due its high-energy consumption; therefore, it should be used as a last resort.

In the following sections, the operation of each system is shown and considers a particular day of the year, which is not essentially the same for the different systems. This approach is necessary to illustrate all operation modes in one single day. All of the operation modes described in the following sections assume temperature schedule 1, except when defined otherwise.

4.1 ASHP

As seen in Fig. 1a, the ASHP scheme is the simplest configuration analyzed. An air-to-water heat pump is connected to the pool and delivers hot water with circuit 9–10–11–12, which has an auxiliary heater installed in series. Therefore, there are two operation modes: heat pump only and heat pump combined with an auxiliary

Table 3 Set-point temperature schedules considered to control the pool temperature

	Period 1 0 to 8 AM	Period 2 8 AM to 6 PM	Period 3 6 PM to 0 AM
Schedule 1 (°C)	24	28	28
Schedule 2 (°C)	24	28	24

Table 4 Thermostat set points and dead bands

Equipment	Set-point temperature	Dead band (°C)
Heat pump	$T_{p,set}$ = Set-point schedule	4
Solar collector	$T_{valve,set} = T_{p,set} + 1$	3
Auxiliary heater	$T_{aux,set} = T_{p,set}^{-3}$	2

heater. A two-stage thermostat controls these operation modes. The first stage, which controls the heat pump, has a temperature set point of $T_{p,set}$, and the second stage, which controls the auxiliary heater, has a temperature set point of $T_{aux,set}$. Both controllers consider a dead band, as defined in Table 4.

Figure 2 shows the operation of the ASHP system for September 9. At the beginning of the day, the water temperature of the pool was above that of the set point. Therefore, the system was not in operation. At 8:00 am, the pool set-point schedule shifts to 28 °C, because the pool is at approximately 24 °C. Below the set point minus half of the dead band (26 °C, the heat pump is turned on. Because the water pool temperature is also below the auxiliary heater set point, this device is also turned on. This can be noted by the mass flow rate in the evaporator ($\dot{m}_e$) and condenser ($\dot{m}_c$) and by the high increase in the outlet temperature of the auxiliary heater ($T_{heat,o}$).

The auxiliary heater operates until the pool temperature reaches 26 °C at 12:00 noon. From this point onward, the heat pump continues operating until the end of the day. Because the heat pump cannot heat the pool to the set-point temperature plus half of the dead band (30 °C) by the end of the day, the pool only reaches a temperature of 24 °C and the auxiliary heater is briefly turned on.

It can been seen that the temperature difference between the inlet and outlet of the evaporator ($T_{amb} - T_{e,o}$) is approximately constant (8 °C). This is due to the increase in the air mass flow rate in the evaporator, which is internally controlled by the heat pump as the ambient temperature decreases.

4.2 SA-ASHP

The only difference between the SA-ASHP system and the reference case is the solar loop connected in parallel to the heat pump, as shown in Fig. 1b. The air-to-water heat pump and the auxiliary heater deliver the water with circuit 9–10–11–12–16–17, while the bypass valves connect the solar field directly to the pool with circuit 9–13–14–15–16–17. This system has two basic operation modes: heat pump and direct solar heating. In addition, the auxiliary heater can operate as a complementary heating device for both of these modes.

The heat pump and the auxiliary heater are controlled by the same scheme used for the ASHP system. The bypass circuit is controlled by an on/off differential controller with upper and lower dead bands set at 2.5 and 0.5 °C, respectively. Naturally, the use of solar energy for pool heating purposes is preferred over the heat pump. When the solar irradiance is high enough to maintain the desired temperature, the heat pump is shut off. The hierarchy between the controllers was implemented using Boolean algebra.

Figure 3 shows the operation of the SA-ASHP system for April 3. As in an ASHP system, the pool starts the day heated, and the heating system is off. At 8:00 am, when the set-point schedule shifts to 28 °C, the heat pump is turned on. This is because the pool temperature was approximately 25 °C, which is a value that is below the set-point temperature minus half of the dead band (26 °C). At approximately 10:00 am, the heat pump is shut off due to the temperature of the water flow coming from the solar collectors ($T_{col,o}$) that is 2.5 °C higher than the pool temperature (T_p). Thus, the solar direct heating circuit is used to heat the pool until approximately 16:00 pm, which is depicted by the solar collector mass flow rate ($\dot{m}_{col}$) observed in Fig. 3. At this moment, the solar field cannot provide water at a

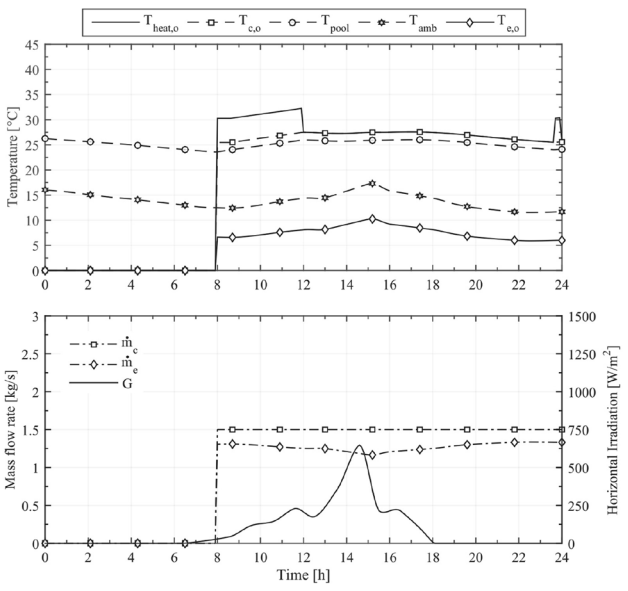

Fig. 2 Daily variation of the operating temperatures, mass flow rate and solar irradiation of the ASHP system, for September 9

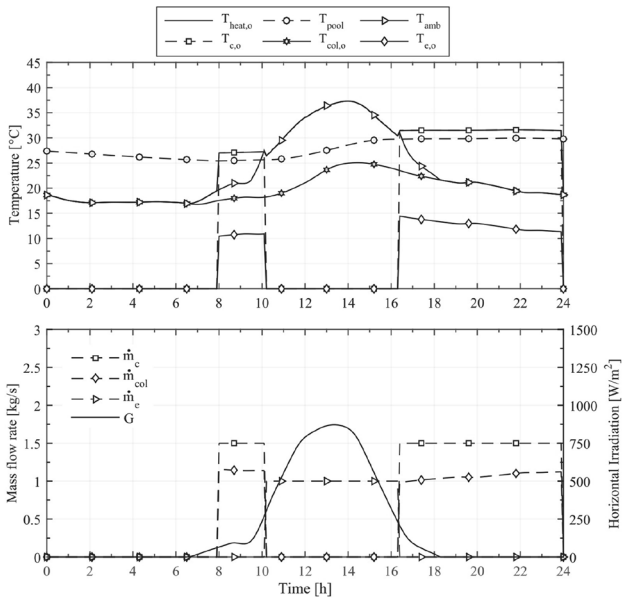

Fig. 3 Daily variation of the operating temperatures, mass flow rate, and solar irradiation of the SA-ASHP system, for April 3

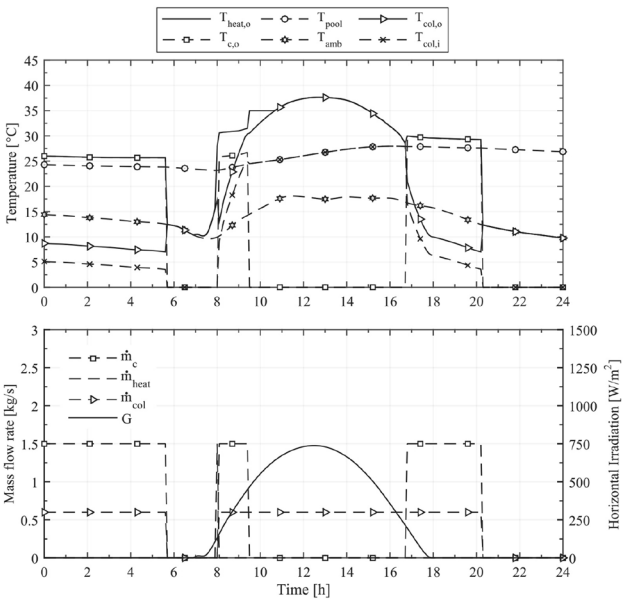

Fig. 4 Daily variation of the operating temperatures, mass flow rate and solar irradiation of the SA-WSHP system, for August 10

temperature above the pool temperature. From this time to the end of the day, the pool is heated by the heat pump because the pool water temperature only reaches the shut off temperature (30 °C) close to midnight.

4.3 SA-WSHP

For this system, a water-to-water heat pump is considered, as shown in the schematic diagram in Fig. 1c. The solar collectors can work as a heat source for the heat pump (circuit 8–18–19–20–7), and then the heat pump heats the pool with circuit 9–10–11–14–16–22–23 or by directly heating the pool with the circuit (9–17–18–19–20–21–22–23). When the solar field cannot supply the heat load to the heat pump or directly to the pool, the auxiliary heater supplies the load with circuit 9–10–11–14–16–22–23. Hence, SA-WSHP has only three basic operation modes: heat pump, direct solar heating, and auxiliary heater. However, the auxiliary heater can work as a complementary device for the heat pump and direct solar heating.

The controller of this system is far more complicated than the previous controllers. There are five control signs that are combined to properly control the equipment. In addition to the three control signs used in the SA-ASHP scheme (two thermostats and one differential controller), it is necessary to include a controller to shut off the heat pump to avoid frosting problems in the solar collector water loop (8–18–19–20–7) and an additional thermostat controller to activate the solar direct heating circuit. These two additional controllers are necessary because the water source heat pump feeds chilled water to the solar field. Consequently, the solar field could absorb heat from the ambient when the collector temperature is below the ambient air temperature, thus allowing the heat pump to operate even at night. Therefore, the on/off differential controller (used in the SA-ASHP system) is not sufficient to control the bypass valves once the solar field could absorb heat from the ambient. Hence, the bypass valves are activated when the water flow temperature from the solar collectors reaches $T_{\text{valve,set}}$. The anti-frost controller shuts off the heat pump if the water flow temperature from the evaporator is lower than 4 °C, and it turns on as the water flow temperature reaches 18 °C.

Figure 4 shows the operation of SA-WSHP for August 10. Because the heating demand was not met during the previous day, the day starts with the heat pump operating. The water source heat pump can operate overnight because it feeds chilled water to the solar field and, consequently, it absorbs heat from the ambient by convection. Between 0 and 6 am, the heat pump feeds water at a temperature of approximately 5 °C to the solar field. Because this temperature is below the ambient temperature ($T_{\text{amb}} = 15$°C), the solar field can absorb heat from the ambient and deliver water at approximately 8 °C. Although the temperature increase is only 3 °C, it allows the operation of the heat pump, evidenced by the water mass flow rate in the condenser ($\dot{m}_c$) and in the solar collectors ($\dot{m}_{\text{col}}$).

For approximately 6 h, the water flow temperature from the solar field reaches 7 °C and the heat pump is shut off due to the anti-frost controller. Because the pool

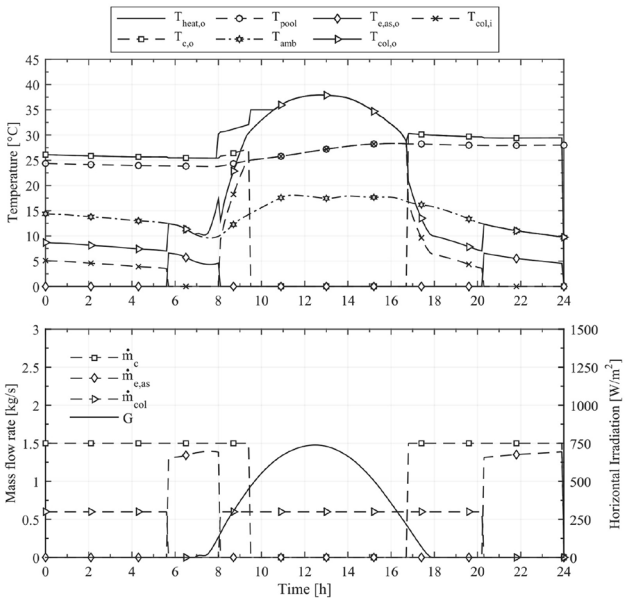

Fig. 5 Daily variation of the operating temperatures, mass flow rate and solar irradiation of the SA-DSHP system, for August 10

temperature was approximately 24 °C, the auxiliary heater was disabled.

Once again, at 8 am, the pool temperature set-point schedule shifts to 28 °C, so from this time the water temperature is below the temperature set points for the heat pump and the auxiliary heater. Therefore, both devices begin their operation. This is depicted in Fig. 4 by the water mass flow rate in the condenser ($\dot{m}_c$) and in the solar collectors ($\dot{m}_{col}$). The abrupt increase in the water temperature from the auxiliary heater indicates its operation. In addition to the aforementioned effects, between 8 to 10 am, the solar radiation heats the water flowing in the solar field, thus increasing the performance of the heat pump.

At approximately 9:30 am, the outlet water temperature of the solar collectors ($T_{col,o}$) reaches the set point and the bypass valves are activated. Then, the pool is heated directly by the solar collectors. From 8 to 11 am, the auxiliary heater is operated as a supplementary source. However, as the water pool temperature reaches 26 °C, this device is disabled.

The solar direct heating operates until approximately 17:00, which is the moment that the solar field could not provide sufficient heat to increase the temperature of the pool. Because the pool still demands heat, the water source heat pump starts its operation by absorbing energy from the solar field. At approximately 20:00, the outlet water temperature of the solar collectors ($T_{col,o}$) reaches 7 °C, and the heat pump is disabled for anti-freezing protection.

Table 5 Annual results obtained for the reference system designs

System	ASHP	SA-ASHP	SA-WSHP	SA-DSHP
F (%)	76.6	86.8	85.0	87.8
$\overline{COP}$ (–)	4.9	4.8	6.3	6.1
SPF (–)	4.3	7.6	6.7	8.2
F_{aux} (%)	3.8	2.9	6.0	2.0
F_{hp} (%)	19.7	10.3	9.0	10.2
$F_{l,direct}$ (%)	–	47.7	36.7	35.3
$F_{l,wshp}$ (%)	–	–	56.9	57.6
$F_{l,ashp}$ (%)	96.0	49.0	–	5.0
Q_L (MWh)	37.1	39.2	39.7	39.9

4.4 SA-DSHP

SA-DSHP consists of a heat pump with two evaporators in parallel. One of these evaporators is an air-to-refrigerant type, and the other evaporator is a water-to-refrigerant heat exchanger, as shown in Fig. 1d.

The SA-DSHP system operates similar to the SA-WSHP system. The solar field heats the pool directly with circuit 9–13–14–15–16–17–18–19 and works as a heat source for the water evaporator of the heat pump with circuit 8–14–15–16–7. The heat pump heats the pool with circuit 9–10–11–12–15–19. However, when the heat pump needs to be shut off due the water anti-freeze controller, the internal valves actuate and the air heat exchanger is used as the evaporator. Consequently, SA-DSHP has three basic operation modes: heat pump with water evaporator, heat pump with air evaporator, and direct solar heating. As for the other configurations, in all of the operating modes, the auxiliary heater can supply the complementary heat demanded.

The controllers used in the SA-DSHP system are identical to those used in the SA-WSHP system, with an additional anti-freeze controller, which activates the air evaporator as a heat source, instead of shutting off the heat pump.

Figure 5 presents the operation of the SA-DSHP system for August 10. Between 0 and 5:30 am, the solar field is used as a heat source for the water evaporator, as evidenced by the water mass flow rate circulating in the solar collectors.

At approximately 5:30 am, the outlet water temperature of the solar collectors ($T_{col,o}$) reaches 7 °C and the water source evaporator was disabled for anti-freezing protection. At this moment, the dual-source heat pump uses the air evaporator and the heating process continues. This is observed by the air mass flow rate in the evaporator ($\dot{m}_{e,as}$) and the outlet air temperature in the evaporator ($T_{e,as,o}$). At approximately 8 am, the solar field absorbs sufficient solar radiation to provide water at a temperature suitable for

operating the heat pump, so the water evaporator is activated again.

As soon as the outlet water temperature of the solar collectors ($T_{col,o}$) reaches the valve set-point temperature, the bypass valves are activated and then the pool is heated directly by the solar collectors. This effect is shown by the curve of the water mass flow rate in the solar collectors ($\dot{m}_{col}$), observed between 10 am and 16 pm.

Near sunset, the solar field cannot heat the pool directly. Therefore, the heat pump is turned on with the water source evaporator. This mode of operation is maintained until 20:00 pm, when anti-freezing protection is triggered and starts using the air source evaporator. Because the pool water temperature never reaches the set-point (including the dead band), the heating system operates all day.

5 Results

The annual results obtained for the reference system are shown in Table 5. The non-purchased energy fraction of the four systems varies from 76 to 88%. In other words, only 12–24% of the energy used to heat the pool is purchased.

The energy consumption fraction of the auxiliary heater is between 2 and 6% of the pool's thermal load, where the SA-WSHP system is the largest consumer of energy. The main reason for that is the restricted operation scheme for absorbing energy from the ambient by the solar field and, consequently, the use of the anti-frost controller. The low values for the energy consumption fraction show that the solar-assisted heat pump cannot completely provide the energy demands for heating the pool. However, because these values are very low, the auxiliary heater could be disabled without a significant reduction in comfort.

For the energy consumption fraction of the heat pumps, it can be noted that the ASHP system has the largest energy consumption, approximately 20% of the total. The solar-assisted systems have an energy consumption of approximately 10%, where the SA-WSHP system shows the lowest consumption, 9% of the total. However, when both consumption fractions ($F_{aux} + F_{hp}$) are considered, SA-DSHP presents the lowest value (12.2%) followed by the SA-ASHP (13.2%), SA-WSHP (15%) and ASHP systems (23.5%). These results show that the integration of solar energy with heat pumps can provide an energy consumption reduction of 44, 36, and 48% compared to the ASHP system for SA-ASHP, SA-WSHP, and SA-DSHP, respectively.

The reduction in energy consumption is due to an increase in the load fraction of direct solar heating ($F_{l,direct}$) and the reduction in the load fraction of the heat pump ($F_{l,ashp}, F_{l,wshp}$). For example, the load fraction for direct solar heating of SA-ASHP is approximately 47%, which results in a decrease in the load fraction of the heat pump ($F_{l,ashp}$) from 96% for the ASHP, to 49% for the SA-ASHP system. The same behavior is observed for the SA-WSHP and SA-DSHP systems. However, the reduction in the heat pump load fraction is approximately 10% lower for these two systems than in the SA-ASHP, due to the low amount of direct solar heating energy used in the SA-WSHP and SA-DSHP systems at approximately 36%, whereas the SA-ASHP has 47%. This is explained by the fact that part of the energy absorbed by the solar field was used as the heat source by the heat pump, as evidenced by the increase in the annual coefficient of performance. The two systems using water source heat pumps present an annual COP of six, while the air source heat pump has a COP of five.

To directly compare the four configurations, a seasonal performance factor SPF for the whole system was calculated. This indicator accounts for the contribution of all operation modes, and therefore it depicts the effects of the integration of solar energy on the reduction in the energy consumption of the system over the complete year. As shown in Table 5, the ASHP system has the lowest value (4.3), which is slightly lower than the $\overline{COP}$ (4.9). This reduction is caused by the use of energy at the auxiliary heater. For the SA-ASHP system, the performance factor is 7.6, which is 77% higher than the performance factor for the ASHP system. This is a direct consequence of using direct solar heating because it reduces both the heat pump electricity consumption and the auxiliary energy consumption.

The SA-WSHP system has an SPF of 6.7, which is slightly lower than the SPF for the SA-ASHP system, even though it is 44% higher than the value obtained for the ASHP system. In turn, the SA-DSHP system has the highest SPF, with a value of 8.2. This represents an increase in performance of 90% versus the ASHP system.

As presented in Table 5, the pool thermal load (Q_L) is practically constant for all configurations with the exception of the ASHP system, which presents a thermal load 5% lower than the others. This result indicates that for the simulated conditions, the water pool temperature will be slightly higher when heated by the ASHP system. Figure 6 depicts a cumulative distribution function of the water pool temperature for the four systems. It can be noted that the ASHP system has slightly lower values for the temperature at the pool. On the other hand, this figure shows that 94% of the time, the pool was between 24 and 30 °C, which agrees with the recommendations of FINA and the American Red Cross. However, for the remaining 6% of the time, the pool was maintained between 30 and 33 °C, which is considerably high and potentially hazardous to health.

Figure 7 shows the breakdown of the annual energy losses and gains of the pool for each system. The losses are represented by the evaporation, convection, long-wave

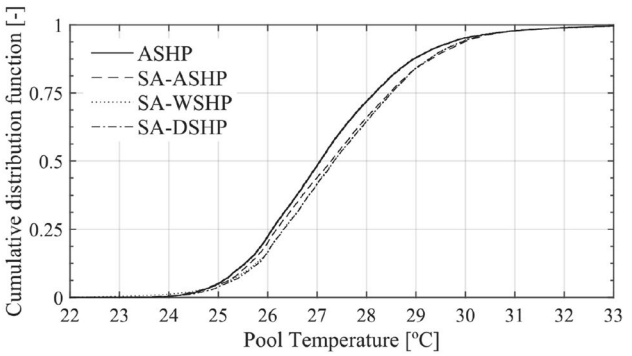

Fig. 6 Cumulative distribution function of the pool temperature for the four systems at reference design

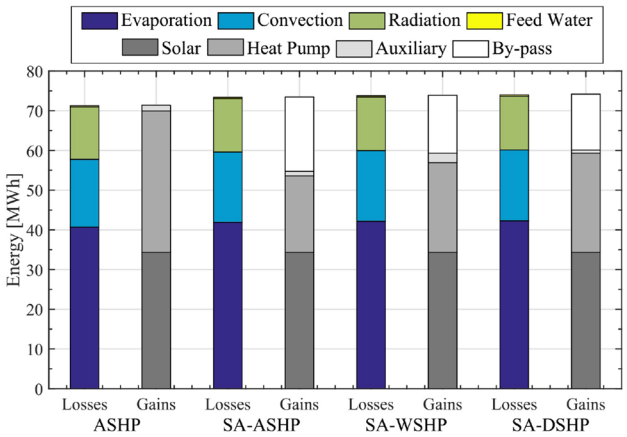

Fig. 7 Energy balance of the system in terms of energy gains and losses for the four systems at reference design

radiation, and freshwater supply. The energy gains are the heat flow with short-wave radiation (passive solar heating), a heat pump, an auxiliary heater, and direct solar heating, where the sum of these last three quantities represents the thermal load of the pool (Q_L). As noted, the energy gains counteract the energy losses by keeping the pool at a constant annual average temperature.

Naturally, because the pool for all cases (systems) has nearly the same conditions, the breakdown of the energy losses is approximately the same for all of the systems analyzed. As observed, approximately 57% of the energy is lost by evaporation, 24% by convection, 18% by long-wave radiation, and less than 1% by freshwater supply. The short-wave radiation gain is equivalent for all systems and represents approximately 47% of the energy gains. Therefore, 53% of the energy gains are supplied by the heating system. As seen in Fig. 7, direct solar heating reduces the contribution of the heat pump and the auxiliary heater, thus reducing the energy consumption of the solar-assisted systems.

The monthly performance of the systems is shown in Fig. 8. For the ASHP system, the load fraction of the heat pump during autumn and winter slightly decreases due to the decrease in ambient temperature. During this period, the auxiliary heater is used to meet the energy requirements of the pool by inducing a reduction on the non-purchased energy fraction that fluctuates approximately 80%. The energy consumption of the heat pump is nearly constant in a monthly base, showing a slight decrease in the winter season.

The monthly performance of SA-ASHP has a higher dependency on the weather; therefore, it varies seasonally. In the spring and summer seasons, the solar direct heating fraction achieves values up to 70%, which reduces the auxiliary load fraction to zero, the heat pump load fraction to 30%, and the heat pump energy consumption fraction to approximately 6%. Therefore, in these seasons, the SA-ASHP system can achieve a non-purchased energy fraction of up to 95%. However, during the autumn and winter seasons, the solar direct heating fraction falls from 50 to 40%, thus increasing the use of the heat pump and the auxiliary heater to meet the pool energy demand. Consequently, the energy consumption fraction of the heat pump and auxiliary heater increases, reducing the non-purchased energy fraction to approximately 80% in winter.

The SA-WSHP and SA-DSHP systems operate in a similar way. During the summer and early autumn season, the solar direct heating fraction achieve values of approximately 50%, without the auxiliary heater and air evaporator in the SA-DSHP system. Thus, the load fraction of the water source heat pump is approximately 50%, with an energy consumption fraction of approximately 9% and, consequently, a non-purchased fraction of up to 91% for both systems, SA-WSHP and SA-DSHP.

In late autumn and winter, the fraction for solar direct heating falls to 30%. The load fraction of the water source

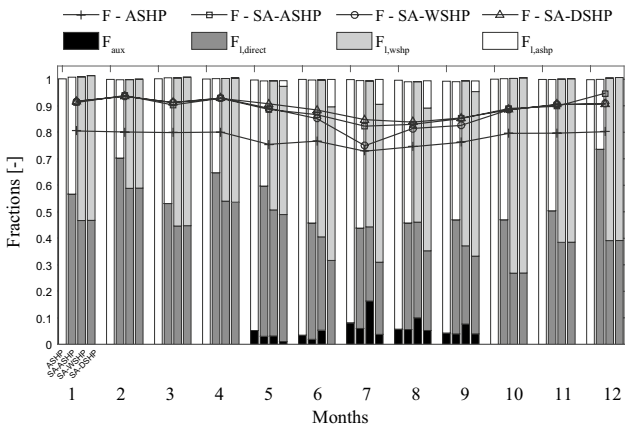

Fig. 8 Monthly performance of the systems at the reference design

Table 6 Scaled heat pump capacity and electrical power at rated condition

	Scale factor (SF)					
	0.4	0.6	0.8	1.0	1.2	1.4
WS-Cap (kW)	4.7	7.1	9.5	11.9	14.3	16.6
WS-Pwr (kW)	0.8	1.2	1.6	1.9	2.4	2.8
AS-Cap (kW)	3.9	5.8	7.8	9.7	11.6	13.6
AS-Pwr (kW)	0.9	1.3	1.7	2.2	2.6	3.1

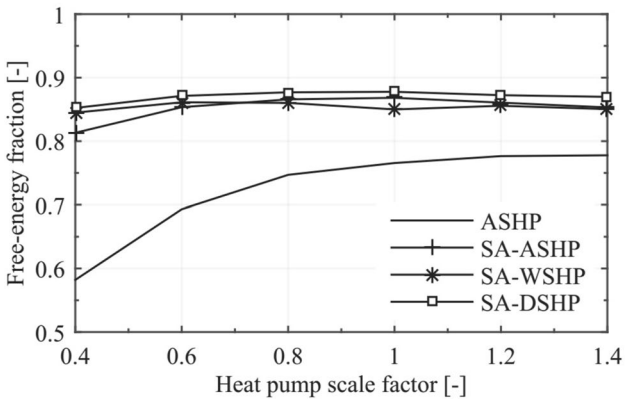

Fig. 9 Free-energy fraction as a function of the heat pump scale factor

heat pump increases to approximately 60%, showing that a considerable part of the solar energy absorbed was used as a heat source for the heat pump. However, this increase was not large enough to supply the total energy requirements of the pool. Therefore, for the SA-WSHP system, the auxiliary heater was extensively used, achieving a consumption fraction between 15 and 10% in July and August, respectively. In turn, in the SA-DSHP system, the air source evaporator was used to complement the heating load that was not met by the water source evaporator. Therefore, the system achieved only 5% of the auxiliary heater consumption fraction in August. As a consequence, SA-DSHP has a smooth non-purchased energy fraction over these months, varying from 95 to 85%, in February and August, respectively. For SA-WSHP, this fraction varies from 93 to 75% in February and July, respectively. During the spring season, both fractions for solar direct heating and the load fraction of the water source heat pump increase, reducing the use of the auxiliary heater in both systems. In addition, this effect reduces the use of the air source evaporator in the SA-DSHP.

5.1 Effect of heat pump capacity

A scale analysis was conducted to analyze the effect of the capacity of the heat pump on the performance of the system. Therefore, rating parameters of the heat pump

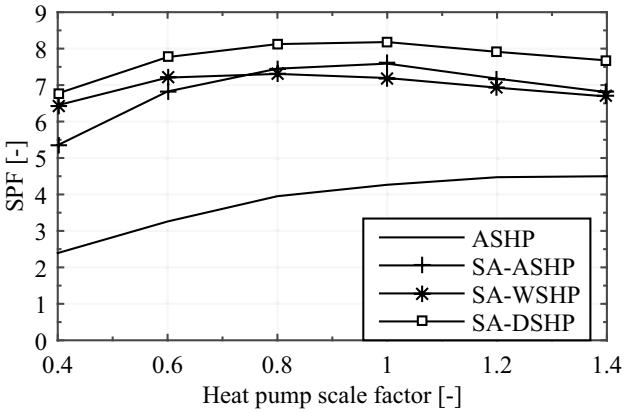

Fig. 10 System seasonal performance factor as a function of the heat pump scale factor

were linearly scaled, as the volumetric displacement rate of the compressor and the valve flow coefficient. The heat pump capacity and power for the water source and for the air source heat pump considered herein are presented in Table 6 as a function of the scale factor (SF).

Figure 9 shows the *F* fraction as a function of the scale factor for the four systems. It can be seen that the *F* fraction of the ASHP systems presents an asymptotic growth with respect to the scale factor for a maximum value of approximately 78%. For the solar-assisted systems, the figure depicts nearly the same non-purchased energy fraction, where the SA-DSHP system shows higher values.

To visualize the system that presents a better performance, the seasonal performance factor as a function of the scale factor is shown in Fig. 10. This figure depicts an optimum value of the heat pump capacity (scale factor) that maximizes the seasonal performance factor and minimizes the energy consumption. The optimum SF value for the SA-ASHP and SA-DSHP systems are approximately one. The SA-WSHP system has an optimum performance for SF of 0.6. This is explained by the use of the solar field to absorb energy from the ambient. When the size of the solar field is fixed, the increase in the capacity of the heat pump can freeze the water loop, which is prevented by the anti-freeze control by turning off the equipment.

On the other hand, the decrease in the SPF values for large heat pump capacities is due to the reduction in the solar direct heating fraction. This reduction in the SPF is not sharp, because the increase in the heat pump capacity also reduces the auxiliary energy consumption, which increases the performance of the system.

5.2 Effect of the solar field

The effect of the solar field was analyzed with respect to two parameters: the solar field area and the collector

efficiency. The last parameter was analyzed by varying the collector heat loss parameter $F_R U_L$, while the optical efficiency was maintained constant. The seasonal performance factor was chosen as a performance indicator because it quantifies the overall performance of the system in terms of the solar, heat pump, and energy consumption shares. Naturally, the performance of the ASHP system is independent of the solar field; however, the results of this system are presented within the next analysis as a reference.

Figure 11 shows the seasonal performance as a function of the $F_R U_L$ parameter. As expected, the SA-ASHP system presents a decrease in the performance due to the decrease in the efficiency of the collectors. On the other hand, the SA-WSHP system has an increase in the SPF with a decrease in the efficiency. This counterintuitive result is explained as due to the use of the solar field to absorb energy from the ambient by convection. Although reducing the efficiency of the solar collector will decrease the solar direct heating fraction, the overall performance of the system increases. Therefore, the use of unglazed collectors with a lower efficiency and high thermal conductivity can increase the performance of the SA-WSHP system. This behavior also supports the DX-SAHP concept, which uses a two-phase flow solar collector to evaporate the refrigerant fluid directly, so it develops better performance than the indirect solar-assisted heat pumps.

SA-DSHP presents a behavior similar to SA-ASHP and SA-WSHP systems. From 12 to 24 W/(m^{2}K), the SPF decreases similar to the SA-ASHP system. However, beyond that point, the dual-source system behaves similar to the SA-WSHP system and the SPF slightly increases.

The effect of the solar field area is presented in Fig. 12. As expected, the SPF of the three solar-assisted systems has an asymptotical growth with the solar field area, showing a maximum value of 10 for the SA-WSHP and a maximum value of 11 for the SA-ASHP and SA-DSHP systems.

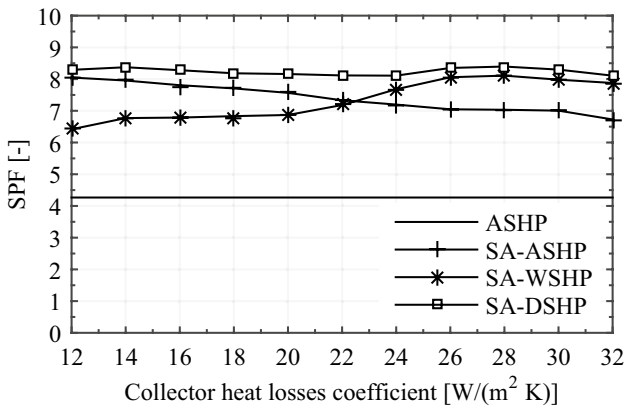

Fig. 11 System seasonal performance factor as a function of the collector heat losses coefficient

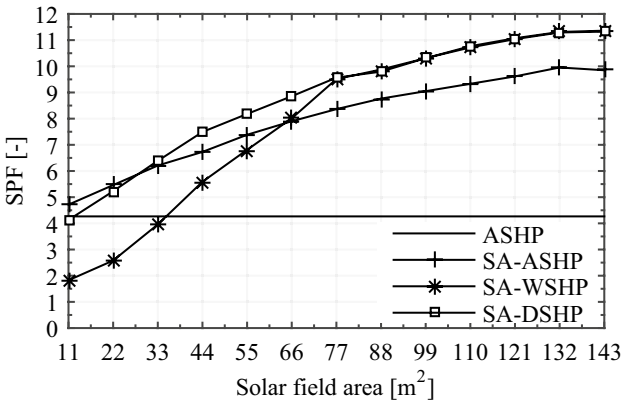

Fig. 12 System seasonal performance factor as a function of the solar field area

It is worth mentioning that when the solar field is neglected, the SA-ASHP and SA-DSHP systems behave similarly to the ASHP system and present the same performance. Consequently, the SPF is approximately four. On the other hand, for small solar fields, the SPF of SA-WSHP approaches the unit, because it will behave similarly to an auxiliary heater system.

There are three important points that should be highlighted in Fig. 12. With a 33 m^2 solar field area, SA-DSHP starts to develop a better performance than SA-ASHP, which is explained by the increase in the COP for the water source heat pump fed with hot water from the solar field. At this point, the SA-ASHP and SA-DSHP systems present an SPF that is 50% higher than the ASHP system. At 66 m^2 solar field area, SA-WSHP has the same SPF value as the SA-ASHP system. Finally, at 77 m^2, SA-WSHP develops the same performance as the SA-DSHP system showing an SPF value of 9.5. These results indicate that when the cost of additional solar field area compensates the additional cost of acquiring a dual-source heat pump, SA-WSHP is a feasible solution. When considering a medium-to-large solar field, the SA-DSHP only performs 10% better than the SA-ASHP system, which probably does not compensate for the additional cost of the system. Yet, for a solar field of equivalent area than the pool (36 m^2), SA-ASHP holds an SPF of 6.5, which represents an increase of 62.5% with respect to the ASHP system.

5.3 Temperature control scheme

This section presents the results for the second set-point temperature schedule defined in Table 3. In this case, the water pool is maintained at approximately 28 °C only during sun hours between 8 am and 6 pm. Therefore, the heating demand will be concentrated during the irradiation

Table 7 Annual results obtained for the modified control strategy

System	ASHP	SA-ASHP	SA-WSHP	SA-DSHP
F (%)	65.8	83.7	82.7	84.0
$\overline{\text{COP}}$ (–)	5.0	4.8	6.7	6.6
SPF (–)	2.9	6.1	5.8	6.2
F_{aux} (%)	18.0	10.4	11.5	9.7
F_{hp} (%)	16.2	5.9	5.8	6.3
$F_{\text{l,direct}}$ (%)	–	60.0	48.5	48.0
$F_{\text{l,wshp}}$ (%)	–	–	39.3	39.3
$F_{\text{l,ashp}}$ (%)	80.8	28.6	–	2.1
Q_{L} (MWh)	34.1	37.1	36.9	37.1

hours. The annual results obtained for this case are presented in Table 7. As observed, the pool thermal load (Q_{L}) is reduced to approximately 6%, indicating a decrease in the average pool temperature. In addition, the fraction for solar direct heating is approximately 60% for the SA-ASHP system and approximately 48% for the SA-WSHP and SA-DSHP systems, which is a 10% increase when compared to the first schedule considered.

The overall performance of the systems using the second schedule is considerably lower than those obtained for the first schedule. For example, the SPF of SA-DSHP was approximately 8.2 and for the second schedule this value was reduced to 6.2, due to the significant increase in energy consumption by the auxiliary heater, as indicated by F_{aux}. The increase in the auxiliary heater's use occurs because the pool cools down during the night and reaches close to 24 °C. Therefore, when the set-point schedule shifts to 28 at 8 am, the pool temperature is below the auxiliary heater set-point temperature ($T_{\text{aux,set}}$), thus enabling its operation. However, if the users accept a less restricted temperature control, the auxiliary heater set-point temperature could be reduced. This action induces a reduction in the auxiliary energy consumption fraction to values similar to those observed in Table 5.

5.4 Economic analysis

To assess the proposed system, an economic analysis was developed, based on the life cycle savings (LCS) method. This analysis allows to evaluate the configurations in terms of solar collector area and heat pump capacity. The P_1 and P_2 method was chosen as recommended by [7]. The LCS is expressed as follows:

$$\begin{aligned} LCS = &\left[(1-F_{\text{aux}})C_{F,\text{aux}}P_{1,1}\right. \\ &\left.-F_{\text{hp}}C_{F,\text{ele}}P_{1,2}\right]Q_{\text{L}} \\ &-\left[(1+C_{\text{inst},A})C_{\text{A}}A_c\right. \\ &\left.+(1+C_{\text{inst,hp}})C_{\text{hp}}+C_E\right]P_2 \end{aligned} \tag{19}$$

where $C_{F,\text{ele}}$ and $C_{F,\text{aux}}$ are the tariff of the electricity and auxiliary heater fuel (natural gas). $P_{1,1}$ is the P_1 term for the natural gas, and $P_{1,2}$ is the P_1 term for the electricity. $C_{\text{inst},A}$ and $C_{\text{inst,hp}}$ are the installation cost of the solar field and heat pump, as a percentage of the acquisition cost of the solar field and heat pump, respectively. C_{A} is the area-dependent cost, A_c the solar field area, C_{hp} the heat pump cost and C_E the auxiliary heater cost. Additionally, the following considerations were adopted for the P_1 and P_2 methods: no income is produced, no loan or financing schemes are considered for the initial investment, and no net property tax cost is produced. The equipment cost and economic consideration are presented in Table 8, as a representative scenario of the current Brazilian market.

It is worth mentioning that the air source and the water source heat pumps have the same initial cost, which can be expressed as a function of the scale factor,

$$C_{\text{hp}} = 1425.07\text{SF} + 1652.9 \tag{20}$$

For the dual-source heat pump, a cost 20% higher than that considered for the air and water-source heat pumps was specified.

The LCS method was applied varying the solar field size, for each heat pump capacity and configuration. However, Fig. 13 depicts only the trade-off curves for the optimum heat pump capacity. Naturally, the ASHP configuration presents a horizontal LCS line and an optimum heat pump scale factor of 1.4. For the SA-ASHP configuration, a maximum LCS of approximately 99 m^2 with a heat pump scale factor of 0.8 is observed. On the other hand, SA-WSHP presents high negative values of the LCS for small solar fields, with a maximum LCS for a solar field higher than 143 m^2 , impractical for residential applications. Finally, SA-DSHP achieves a maximum LCS value

Table 8 Economic considerations adopted

Parameter	Value
Period of economic analysis, N_{e}	20 years
Insurance and maintenance cost, M_{s}	1%
Discount rate, d	7.25%
Inflation rate of fuels, I_{F}	5%
Resale value, R_{v}	10%
Electricity tariff, $C_{F,\text{ele}}$	0.17 US$/kWh
Natural gas tariff, $C_{F,\text{aux}}$	1.293 US$/m^3
LHV of natural gas	39 MJ m^3
Natural gas heater efficiency	80%
Natural heater cost (34 kW), C_E	994.8 US$
Area-dependent cost, C_A	45.2 US$ m^3
Solar field installation cost, $C_{\text{inst,A}}$	10%
Heat pump installation cost, $C_{\text{inst,hp}}$	30%

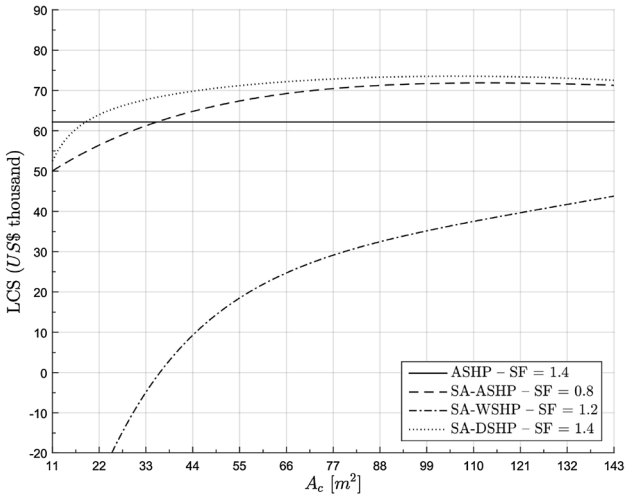

Fig. 13 Life cycle saving as a function of the solar field area

at approximately 99 m^2 of the solar field, with a heat pump scale factor of 1.4. It is worth mentioning that SA-ASHP and SA-DSHP configurations present economic viability and higher LCS than the ASHP configuration.

6 Conclusions

The present study reports a methodology for building and simulating different configurations of swimming pool heating systems, using solar-assisted heat pumps. All operation modes are successfully demonstrated by the operation temperature and mass flow profiles for typical days. In addition, the global energy balance of the system and the energy balance in the heating loop were presented. Therefore, the simulation platform is considered valid because the individual models (Types) were experimentally validated in previous studies, and the heat pump models achieved deviations similar to those found in the technical literature.

The simulation results indicate that the solar-assisted heat pump systems can achieve significantly better performance than a conventional heat pump system. The proposed systems can reduce the energy consumption up to 48%, presenting a seasonal performance factor between 6.7 and 8.2.

An interesting finding of this work is that the performance of the SA-WSHP and SA-DSHP systems increases when combined with low efficiency solar collectors (high values of $F_R U_L$). Some of the insight gained from these results is the possibility of operating the solar collectors as heat exchangers during dawn. Furthermore, by increasing the loss parameter of the solar collector, the system performs as a direct expansion solar-assisted heat pump (DX-SAHP), which generally has a better performance than an indirect system.

In addition, the performance of the system increases considerably with the solar field area as expected in solar systems. However, it was also shown that with large solar field areas, the SA-WSHP and SA-DSHP systems perform identically and the SPF values are higher than those estimated for the SA-ASHP systems. The heat pump capacity also has an important influence on the overall performance, showing a capacity that maximizes the SPF (and minimizes energy consumption). Therefore, a proper design must consider a detailed economic assessment, combining the cost and performance of all of the system components. Considering the current Brazilian context, the economic analysis shows that only the SA-ASHP and SA-DSHP configurations have financial benefits when the solar field is approximately 99 m^2.

Acknowledgements The authors wish to express their gratitude to the Brazilian CNPq (National Counsel of Technological and Scientific Development) for partially funding the present work through a scholarship from Allan Starke. The authors also appreciate the financial support from project Fondecyt N^o 11140725 of the Chilean CONICYT.

References

1. American Red Cross (2014) Water Safety Instructor's Manual—American Red Cross Swimming and Water Safety program, Washington, USA
2. Auer T (1996) Trnsys-Type 144: assessment of an indoor or outdoor swimming pool. TRANSSOLAR-Klimaengineering, Stuttgar, Germany
3. Chow TT, Bai Y, Fong KF, Lin Z (2012) Analysis of a solar assisted heat pump system for indoor swimming pool water and space heating. Appl Energy 100:309–317
4. Chua KJ, Chou SK, Yang WM (2010) Advances in heat pump systems: a review. Appl Energy 87(12):3611–3624
5. Day AR, Karayiannis TG (1994) Solar-assisted heat pump research and development. Build Serv Eng Res Technol 15:71–80
6. Domanski PA, Mclinden MO (1992) A simplified cycle simulation model for the performance rating of refrigerants and refrigerant mixtures. Int J Refrig 1(2):81–88
7. Duffie JA, Beckman WA (2006) Solar engineering of thermal processes, 3rd edn. Wiley, New York
8. European Parliament (2012) Directive 2012/27/EU of the European Parliament and of the Council of 25 October 2012 on energy efficiency. Off J Eur Union Dir, pp 1–56
9. FINA (2013) Fina facilities rules 2013–2017. Federation Internationale de Natation, Laussane, Switzerland
10. Freeman TL, Mitchell JW, Audit TE (1975) Performance of combined solar-heat pump systems. Solar Energy 22:125–135
11. Hahne E, Kubler R (1994) Monitoring and simulation of the thermal performance of solar heated outdoor swimming pools. Solar Energy 53(1):9–19
12. Hepbasli A, Kalinci Y (2009) A review of heat pump water heating systems. Renew Sustain Energy Rev 13(6–7):1211–1229

13. IEA (2013) Energy efficiency market report 2013. International Energy Agency, Paris
14. Jin H, Spitler JD (2002) A parameter estimation based model of water-to-water heat pumps for use in energy calculation programs. ASHRAE Trans 108(1):3–17
15. Klein SA et al (2010) TRNSYS: a transient systems simulation program, V. 17, TESS
16. Klein SA (2015) EES: engineering equation solver, V.10.040-3D, F-chart software
17. Li H., Braun JE, Shen B (2004) Modeling adjustable throat-area expansion valves. In: Proceedings international refrigeration and air conditioning conference at Purdue, 2004, Purdue e-Pubs
18. Liu H, Zhang S, Jiang Y, Yao Y (2015) Simulation analysis of a solar-assisted heat pump system for space heating in severe cold areas. Build Serv Eng Res Technol 36:500–518
19. Ozgener O, Hepbasli A (2007) A review on the energy and exergy analysis of solar assisted heat pump systems. Renew Sustain Energy Rev 11(3):482–496
20. Patnode AM (2006) Simulation and performance evaluation of parabolic trough solar power plants. M.Sc thesis, University of Wisconsin-Madison, USA
21. Qiao H., Radermacher R, Aute V (2010) A review for numerical simulation of vapor compression systems. In: Proceedings international refrigeration and air conditioning conference at Purdue, 2010, Purdue e-Pubs
22. Ruiz E, Martinez PJ (2010) Analysis of an open-air swimming pool solar heating system by using an experimentally validated TRNSYS model. Solar Energy 84(1):116–123
23. SWERA (2013) Solar and wind energy resource assessment. http://en.openei.org/wiki/SWERA/Data. Accessed 01 Jan 2016
24. Tagliafico LA, Scarpa F, Tagliafico G, Valsuani F (2012) An approach to energy saving assessment of solar assisted heat pumps for swimming pool water heating. Energy Build 55:833–840
25. Wang Q, Ren B, Zeng ZY, He W, Liu YQ, Xiangguo X, Chen GM (2015) Development of a novel indirect-expansion solar-assisted multifunctional heat pump with four heat exchangers. Build Serv Eng Res Technol 36:469–481
26. Abreu SL, Basto JE, (2001) Coletores solares planos para líquidos - determinação do rendimento térmico - alo solar, (1002) Relatório Técnico - RTTC - 01/01. Florianópolis, LABSOLAR/LEPTEN/UFSC
27. Carrier Corporation (2009) AQUAZONE 50PSW036-360: water-to-water source heat pump with PURON refrigerant (R-410A), New York
28. Scarpa M, Emmi G, De Carli M (2012) Validation of a numerical model aimed at the estimation of performance of vapor compression based heat pumps. Energy Build 47:411–420